DNS AND PIV STUDY OF THE 3D WAKE BEHIND TAPERED CIRCULAR CYLINDERS

Vagesh D. Narasimhamurthy
Dept. of Energy and Process Engineering,
Norwegian University of Science and Technology (NTNU),
NO-7491 Trondheim, Norway
vagesh@ntnu.no

Jan Visscher
Dept. of Marine Technology, NTNU
NO-7491 Trondheim, Norway
jan.h.visscher@ntnu.no

Helge I. Andersson
Dept. of Energy and Process Engineering, NTNU
NO-7491 Trondheim, Norway
helge.i.andersson@ntnu.no

Bjørnar Pettersen
Dept. of Marine Technology, NTNU
NO-7491 Trondheim, Norway
bjornar.pettersen@ntnu.no

ABSTRACT

Three-dimensional wake behind a tapered circular cylinder has been studied at low-Reynolds number (transition in the wake regime) by performing Direct Numerical Simulation (DNS) and at higher Reynolds numbers (transition in the shear-layer regime) by Particle Image Velocimetry (PIV). The taper ratio (75) was constant in both the studies. In the PIV study it was found that increase in aspect ratio increases the number of shedding cells along the span, an effect also reported by Piccirillo and Van Atta (*J. Fluid Mech.*, 1993). Both mode A and mode B were found to co-exist in the same geometry (DNS) but only in a small span of the cylinder. Flow-visualization revealed that the mode A appeared around $Re \approx 200$ and mode B around $Re \approx 250$. Cross-sectional views of mode B in the DNS results revealed the smaller-scale 'mushroom' vortex pair structures, which is remarkably similar to those found by Williamson (*J. Fluid Mech.*, 1996). The wavelength of mode B was found to be $\lambda_Z/D \approx 1$, which is surprisingly close to the experimental value $\lambda_Z/D = 0.98$ found by Williamson (*J. Fluid Mech.*, 1996) in the uniform circular cylinder wake. In the present DNS study it was found that streamwise vorticity ω_x becomes large as vortex dislocation occurs, an effect also observed by Piccirillo and Van Atta (*J. Fluid Mech.*, 1993).

INTRODUCTION

The flow over cylinders involves complex interactions of three shear layers: a boundary layer, a separating free shear layer, and a wake, in the same problem. Depending on the Reynolds number transition-turbulence may occur either in the wake (TrW) or separating free shear layer (TrSL) or in the boundary layer (TrBL) of a cylinder. However, non-uniformities in the inflow or in the cylinder diameter (e.g. tapered cylinders) may produce the above mentioned regimes to exist side by side in the same geometry.

Three-dimensional instabilities in the laminar unsteady wake (L3 regime) of tapered circular cylinders were previously studied by Papangelou (1992), Piccirillo and Van Atta (1993), Vallés et al. (2002) and more recently by Narasimhamurthy et al. (2006). However, the TrW regime for tapered cylinders has had remarkably few investigations in comparison to uniform circular cylinders. Recently Parnaudeau et al. (2007) performed Direct Numerical Simulation (DNS) in the TrW regime with a taper ratio, $R_T = l/(d_2 - d_1) = 40$ (where l is the length of the circular cylinder and d_2 and d_1 denote the diameter of its wide and narrow ends, respectively). The same Reynolds number range was studied by Narasimhamurthy et al. (2007) but with a different $R_T = 75$ and they found that a change in R_T by a factor of two has only a modest effect on the Strouhal number. After a literature survey it was noted that the only available results in the TrSL regime is the hot-wire measurements by Hsiao and Chiang (1998), where they studied the tapered cylinder wake with different taper ratios and in the Reynolds number range $Re_m = 4.0 \times 10^3$ to 1.4×10^4 (based on the mean diameter d_m).

The present DNS computations is aimed at studying the wake in the low-Reynolds turbulent regime (as DNS at higher Reynolds number is beyond the reach of any modern computational facility). However, Particle Image Velocimetry (PIV) provides an opportunity to study the turbulent wake at higher Reynolds number (low Reynolds numbers could not be reached in our test facility due to practical issues). The aim of the present study is not to validate the DNS results with PIV results and vice versa but to

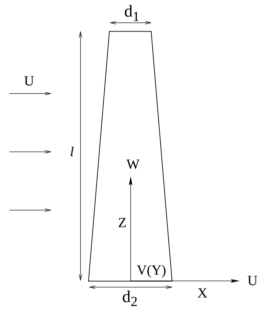

Figure 1: Tapered cylinder configuration

Table 1: Flow parameters ($R_T = 75$).

Case	a	$\mathbf{d_1}$	$\mathbf{d_m}$	$\mathbf{d_2}$	$\mathbf{Re_1}$	$\mathbf{Re_m}$	$\mathbf{Re_2}$
DNS	74	0.34	0.67	1	102	201	300
A_1	13	42	46	50	2100	2300	2500
A_2	13	42	46	50	4200	4600	5000
A_3	13	42	46	50	8400	9200	10000
A_4	13	42	46	50	16800	18400	20000
B_1	26	19	23	27	950	1150	1350
B_2	26	19	23	27	1900	2300	2700
B_3	26	19	23	27	3800	4600	5400

investigate the flow physics in two different Reynolds number ranges with two different techniques (DNS and PIV). It should be noted that the R_T is same in both the cases. Thereby the effect of Reynolds number alone is investigated in the present study.

NUMERICAL AND EXPERIMENTAL SETUP

The tapered cylinder configuration was as shown in figure 1. The aspect ratio ($a = l/d_m$) and the Reynolds numbers Re_2, Re_1, Re_m, based on the uniform inflow velocity ($U = 1$) and the diameters d_2, d_1, d_m, respectively were as shown in Table 1. $R_T = 75$ was constant in all the cases.

The Navier-Stokes equations in *incompressible* form were solved in 3-D space and time using a *parallel* Finite Volume code (Narasimhamurthy et al., 2006; Manhart, 2004). The code uses staggered Cartesian grid arrangement. Time marching was carried out using a 3^{rd} order explicit Runge-Kutta scheme for the momentum equations and an iterative SIP (Strongly Implicit Procedure) solver for the Poisson equation. Spatial discretization was carried out using a 2^{nd} order central-differencing scheme. The total number of grid points used was equal to $15{\times}10^6$. The time step $\Delta t = 0.003 d_2/U$ and the number of Poisson iterations per time step was equal to 50. A uniform inflow velocity profile $U = 1$ was fixed at the inlet without any free-stream perturbations[1]. *Free-slip* boundary condition was applied at the ends of the cylinder. The *no-slip* boundary condition on the cylinder body was implemented by using a *direct forcing* Immersed Boundary Method (Narasimhamurthy et al., 2006; Peller et al., 2006). The total consumption of CPU-time was approximately equal to 12000 CPU-hours on a *SGI Origin 3800* computer.

In the present experimental study stereoscopic PIV was used to measure a large area of the flow field in the cylinder wake with image rates up to 100 Hz. Two different models of same length 600 mm and $R_T = 75$ were used. The mean diameter of the cylinder A is set to 46 mm resulting in an aspect ratio of 13. The mean diameter of the cylinder B is 23 mm, leading to an aspect ratio of 26 (see Table 1). All models were equipped with thin circular end-plates with diameters equal to $3d_{2,A}$ to eliminate disturbances caused by free ends, an effect which has been reported by several authors. An entirely uniform inflow velocity was achieved by towing the models and the measurement system through a still water basin. Each measurement was tailored to observe the maximum number of shedding cycles by estimating the shedding frequency and adapting the image rate to match between 10 and 20 images per cycle. However, the maximum number of images is defined by the camera memory to about 1100 while the maximal experiment length is restricted by the tank length at higher towing velocities. The measurement plane is situated in line with the cylinder axis and directly at its downstream edge. It covers about 400 mm in streamwise and about 300 mm in spanwise direction, thus about half of the cylinder length. To observe the flow along the whole span, each run was repeated for the top, center and lower half. The velocity maps obtained from the images have a resolution of 84 by 72 vectors for all components U, V, and W.

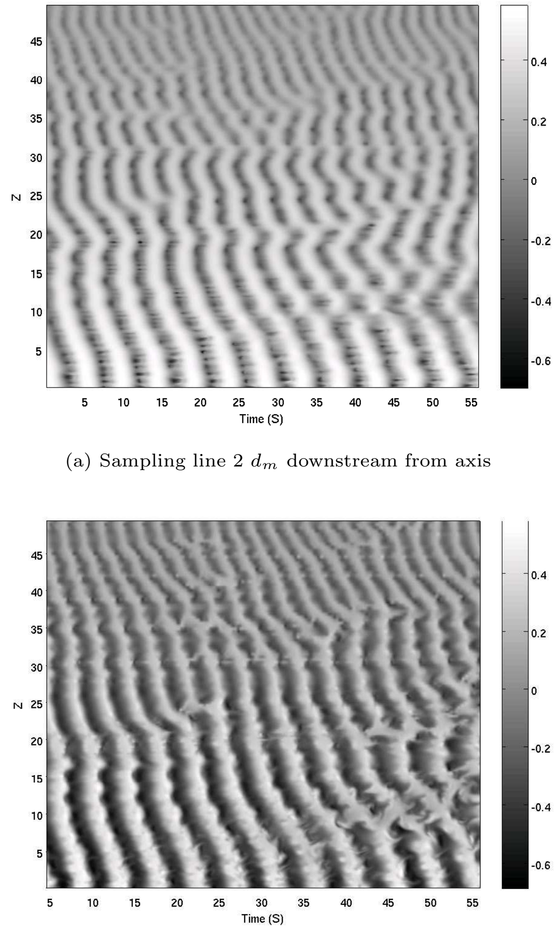

(a) Sampling line 2 d_m downstream from axis

(b) Sampling line 12 d_m downstream from axis

Figure 2: Time evolution of cross-stream velocity 'V' along the span in the present DNS.

[1]Note that transitional wake is still surrounded by laminar free-shear layers and thus insensitive to free stream turbulence.

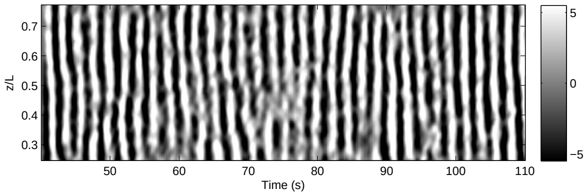

(a) model A_2

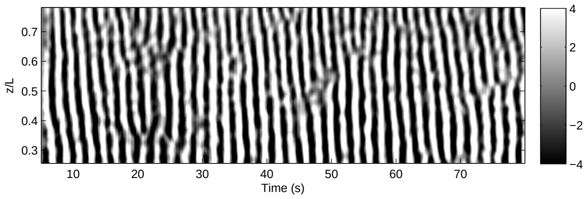

(b) model B_1

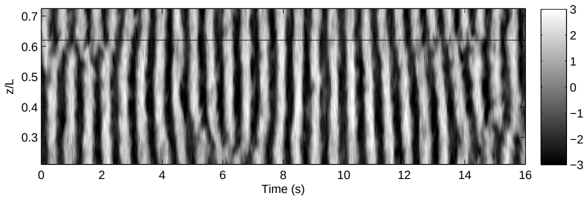

(c) model A_4

Figure 3: Time evolution of 'V' velocity along the span from PIV data (Sampling line 2 d_m downstream from axis).

RESULTS AND DISCUSSION

Figure 2(a),2(b) shows the time evolution of the instantaneous V velocity component in the present DNS sampled along two lines parallel to the axis of the cylinder and located $2d_m$ and $12d_m$ downstream the axis in X-direction, respectively. Similarly, the time evolution from the PIV measurements is shown in figure 3(a),3(b),3(c). An oblique and cellular shedding pattern is evident in both TrW (DNS) and TrSL regime (PIV).

Time traces of the cross-stream velocity (V) signal randomly picked at different Reynolds numbers from the DNS results were shown in figure 4(a),4(b). Low-frequency modulation, a typical feature of *vortex dislocations* or *vortex splits* can be seen in figure 4(a). However, random low-frequency fluctuations, a characteristic feature of TrW state of flow is only visible in figure 4(b) (for $Re > 175$). This is because the transitional eddies are formed laminar but become turbulent as they are carried downstream.

Time traces of U, V, W velocity components inside a dislocation region from the PIV data is shown in figure 5. The U component indicates a frequency modulation and decrease in amplitude similar to the DNS results (figure 4(a)) each time a dislocation occurs. Furthermore, the spanwise W component shows an increased amplitude shortly after. Figure 6 shows the instantaneous flow field of the same case under the vortex split. With the cross-stream V component plotted as background, the vortex centerlines can be found just at the boundary between dark and bright regions. It is obvious that the greatest spanwise velocity appears right in the split zone, while the parallel shedding is dominated by horizontal flow.

Qualitative investigations of the frequency spectra were carried out by the spectral analysis of cross-stream velocity component. The local Strouhal number ($St_{local} = fd_{local}/U$; d_{local} is the local diameter) *versus* local Reynolds number ($Re_{local} = Ud_{local}/\nu$) curve is shown in figure 7.

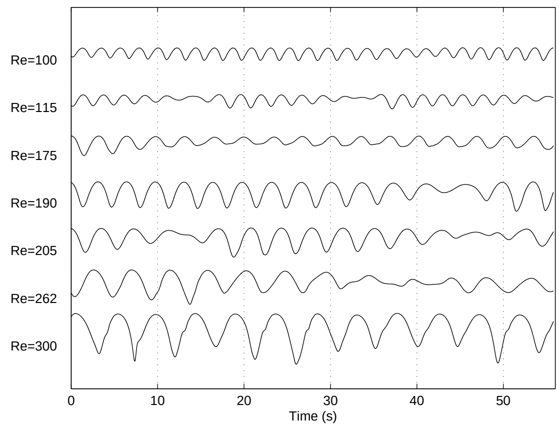

(a) Sampled 2 d_m downstream from axis

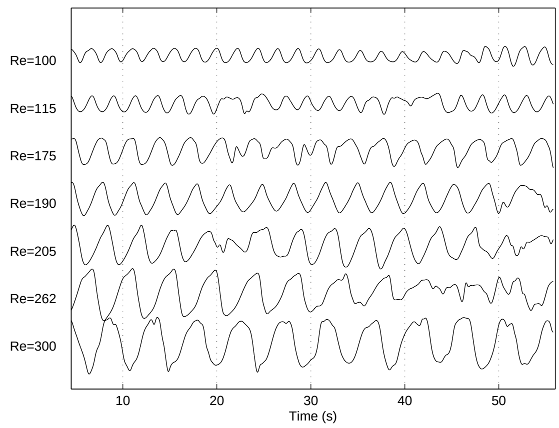

(b) Sampled 12 d_m downstream from axis

Figure 4: Time traces of 'V' velocity (DNS)

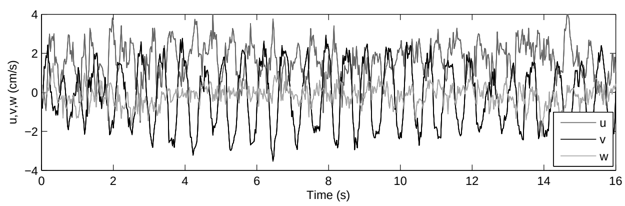

Figure 5: Time traces of U,V,W velocity components along the line marked in figure 3(c). (PIV data)

Piccirillo and Van Atta's (1993) curve-fit ($St = 0.195 - 5.0/Re$) and the numerical results by Narasimhamurthy et al.(2006) for the L3 regime together with the present DNS results (TrW) and the PIV measurements (TrSL) were plotted against the Fey et al. (1998) curve-fit for the uniform circular cylinder. The two discontinuities in the St_{local} *versus* Re_{local} curve in figure 7 for the uniform circular cylinder correspond to change over of eddy-shedding mode from laminar-mode A and mode A-mode B, respectively (Williamson, 1996). In contrast, these vortex dislocations occur spontaneously along the whole span for tapered circular cylinders. The St_{local} *versus* Re_{local} curve for $Re_m > 2300$ from the model B cylinder(PIV) matches the Fey et al. (1998) curve-fit for uniform circular cylinder.

The St_{local} distribution along the span reveals vortex

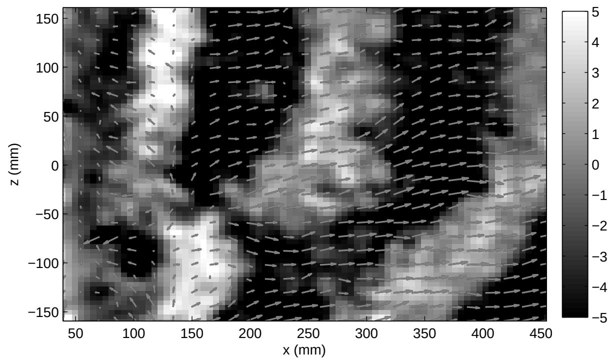

Figure 6: Instantaneous flow field at t=73s for case A_2 (PIV)

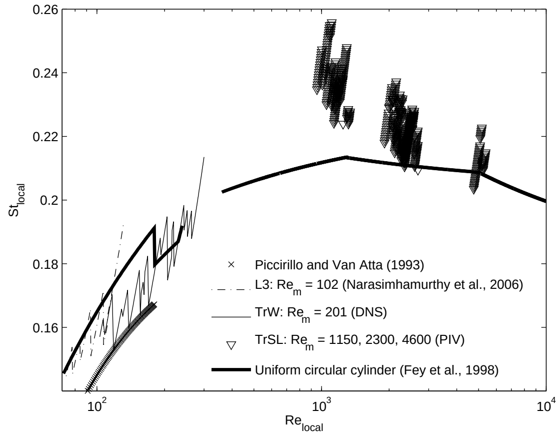

Figure 7: St_{local} *versus* Re_{local}

dislocations as changes in the local shedding frequency (figure 8(a),8(b)). Large jumps in the curve indicate a split region with a fixed spanwise position. If the shedding cell boundaries are more evenly distributed over the span, the St curve shows a greater number of small changes in the shedding frequency. The St_{local} magnitude gets smaller and smaller with increasing Re_m for all the experiments. It is generally lower for the cylinder A. Due to its low aspect ratio, the vortices were hardly dislocated in the model A case. Long time series reveal the presence of two cells with constant shedding frequency for Reynolds numbers up to 4600 (see the single dislocation in figure 3(a)). In the A_3 and A_4 models a third cell appears temporarily at $Re_m > 9200$. Figure 3(c) shows the two splits between the three cells being fixed in spanwise position for case A_4. Increasing numbers of cells with rising Re_m have been reported by Hsiao et al. (1998) as well. Piccirillo and Van Atta (1993) found that increase in aspect ratio increases the number of shedding cells along the span in L3 regime. It is interesting to see a similar effect in the TrSL regime of the present PIV study (see model B results in figure 8(b)). For the B model are the cell boundaries only in the lower half distinct and consistent over multiple experiments. The upper half shows less well defined cell boundaries which is also visible in figure 3(b). This might indicate a stronger end effect on the upper cylinder end.

In order to identify the topology and the geometry of the vortex cores correctly the λ_2-definition by Jeong and Hussain (1995) was used in the present DNS study. λ_2 corresponds to the second largest eigenvalue of the symmetric tensor $S_{ij}S_{ij} + \Omega_{ij}\Omega_{ij}$, where S_{ij} and Ω_{ij} are respectively the symmetric and antisymmetric parts of the velocity gradient tensor. Figure 9 shows the iso-surfaces of negative λ_2, vorticity magnitude or enstrophy $\mid \omega \mid$, streamwise vorticity ω_x and the spanwise vorticity ω_z evaluated at the same instant in time. The vortex dislocations at $Z \approx 12.5, 22, 40$ and the small-scale streamwise structures (mode A and mode B) along the span are clearly visible. The development of helical twisting of vortex tubes is visible in the vicinity of the vortex dislocations. Williamson concluded that these helical twistings are the fundamental cause for the rapid spanwise spreading of dislocations, and indeed for the large-scale distortion and break-up to turbulence in a natural transition wake. In uniform circular cylinder wakes the Reynolds number will be constant along the whole span and therefore the individual modes of 3-dimensionality (either mode A or mode B) exist along the entire span of the cylinder. However, in the present tapered cylinder case (DNS) the Re_{local} varies along the span and both mode A and mode B co-exists in the same geometry. Thereby, only a small span of the cylinder is available for each of the modes to develop (especially for mode A) and it is hard to pin-point the exact Reynolds number at which these modes start to appear. Flow-visualization revealed that the mode A appeared around $Re_{local} \approx 200$ and mode B around $Re_{local} \approx 250$.

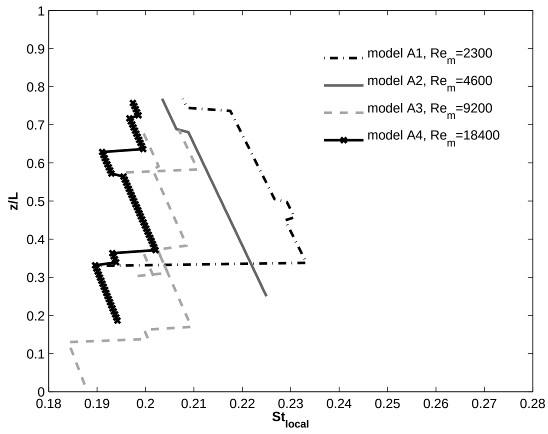

(a) model A; aspect ratio = 13

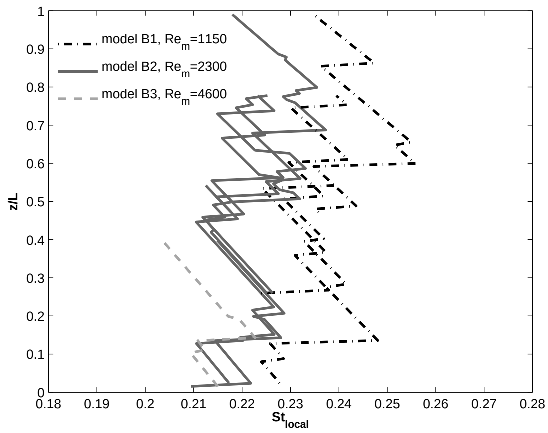

(b) model B; aspect ratio = 26

Figure 8: St_{local} along the span (PIV data)

In figure 10(b),10(c) cross-sectional views of mode-B

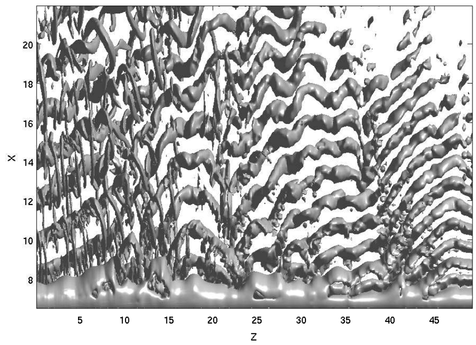

(a) - λ_2

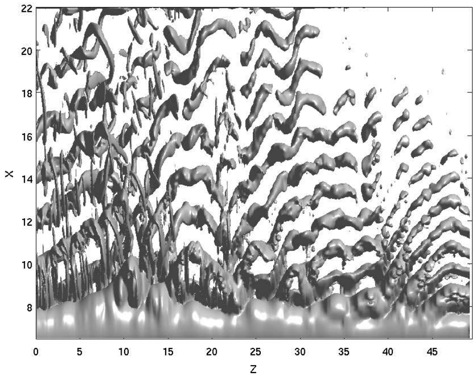

(b) $|\omega|$

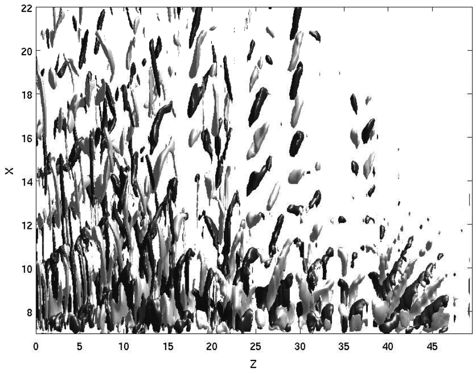

(c) ω_x

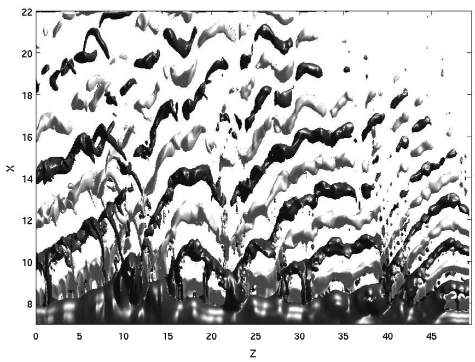

(d) ω_z

Figure 9: 3-dimensional vortical structures from the present DNS taken at the same instant in time as vortex dislocation occurs (at $Z \approx 12.5, 22, 40$) along the span. The flow direction is from bottom to top. (a)Negative λ_2; (b)Enstrophy $\mid \omega \mid$; (c)streamwise vorticity ω_x; (d)cross-stream vorticity ω_z. The surfaces colored white and black mark a particular value of positive and negative vorticity, respectively.

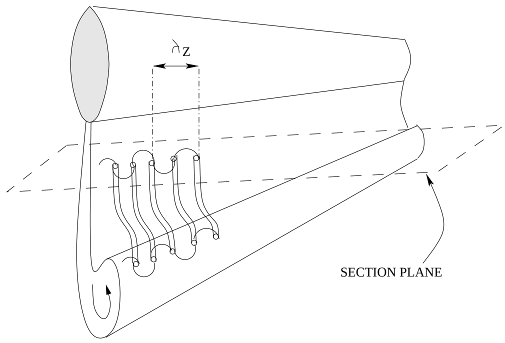

(a) $Y - Z$ section plane (dotted line)

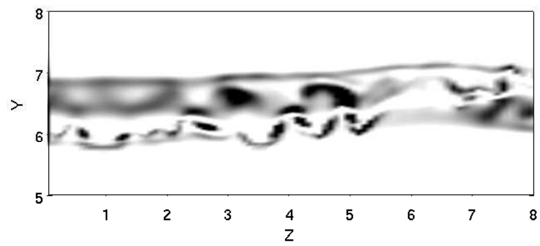

(b) mode B 'mushroom' structures at $Z \approx 3 - 6$

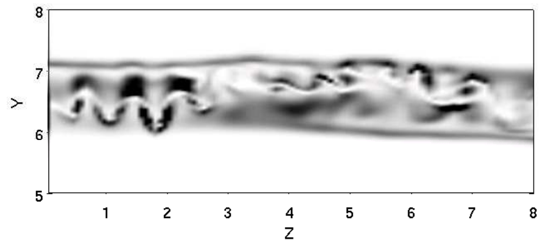

(c) mode B 'mushroom' structures at $Z \approx 0 - 3$

Figure 10: Cross-sectional views of mode B showing 'mushroom' vortex pair structures in the present DNS. (note that section plane is parallel to the axis and at an angle to the vortex lines and thereby structures are visible only in some parts of the plane)

streamwise vortex structure from the DNS results were shown. We can see clearly the smaller-scale 'mushroom' vortex pair structures of mode-B vortex shedding. There is a remarkable similarity between this vortex array and that found by Williamson (1996). However, note that the section plane is parallel to the axis and at an angle to the vortex lines (see figure 10(a)) and thereby structures are visible only in some parts of the plane. The wavelength of mode B was found to be $\lambda_Z/d_2 \approx 1$, which is surprisingly close to the experimental value $\lambda_Z/D = 0.98$ found by Williamson (1996) in the uniform circular cylinder wake.

Piccirillo and Van Atta (1993) reported that the vortex splitting in L3 regime occurs when the streamwise vorticity ω_x becomes too large. It is fascinating to see the sharp contrast between the normal vortex shedding pattern and the vortex split in figure 11(a),11(c) and 11(b),11(d), respectively. Note the increase in ω_x in figure 11(b) and 11(d) by an order of magnitude 10 as vortex splits.

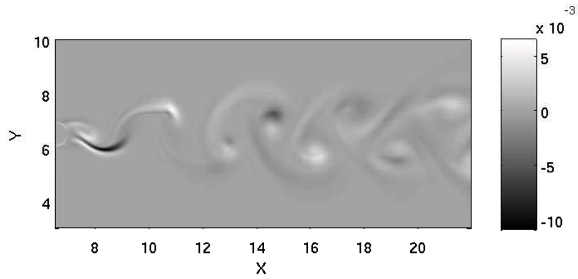

(a) Z=12.5; $Re_{local} = 250$ (before split)

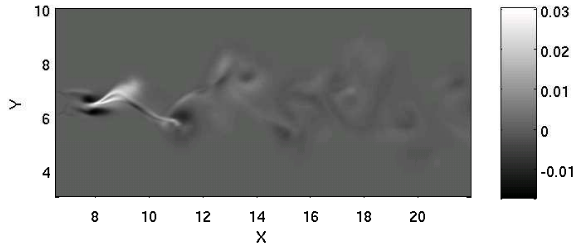

(b) Z=12.5; $Re_{local} = 250$ (vortex split)

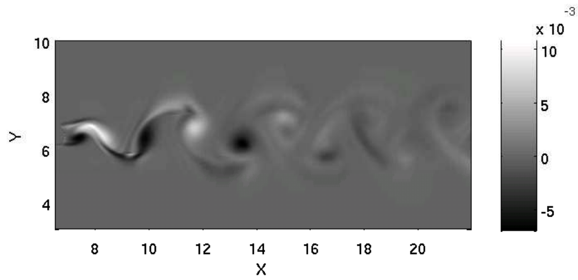

(c) Z=22; $Re_{local} = 212$ (before split)

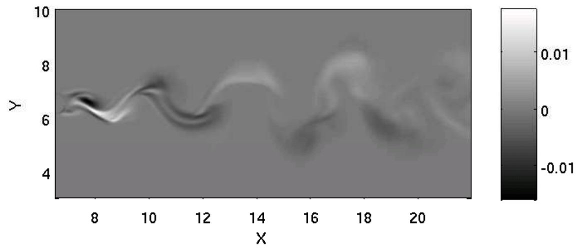

(d) Z=22; $Re_{local} = 212$ (vortex split)

Figure 11: Streamwise vorticity (ω_x) as vortex splits (DNS results). (note that (a),(b) and (c),(d) were taken at the same spanwise location, respectively)

CONCLUSIONS

Oblique and cellular shedding pattern was observed in both TrW (DNS) and TrSL regime (PIV). In the present PIV study it was found that increase in aspect ratio increases the number of shedding cells along the span, an effect also reported by Piccirillo and Van Atta (1993) in their L3 regime case. Both mode A and mode B were found to co-exist in the same geometry (DNS) but only in a small span of the cylinder. Flow-visualization revealed that the mode A appeared around $Re_{local} \approx 200$ and mode B around $Re_{local} \approx 250$. Cross-sectional views of mode B in the DNS results revealed the smaller-scale 'mushroom' vortex pair structures, which is remarkably similar to that found by Williamson (1996). The wavelength of mode B was found to be $\lambda_Z/d_2 \approx 1$, which is surprisingly close to the experimental value $\lambda_Z/D = 0.98$ found by Williamson (1996) in the uniform circular cylinder wake. In the present DNS study it was found that streamwise vorticity ω_x becomes large (increases by an order of magnitude 10) as vortex dislocation occurs, an effect also observed by Piccirillo and Van Atta (1993).

REFERENCES

Fey, U., König, M., and Eckelmann, H., 1998, "A new Strouhal-Reynolds-number relationship for the circular cylinder in the range 47<Re<2 × 10^5", *Phys. Fluids*, Vol. 10, pp. 1547-1549.

Hsiao, F., and Chiang, C., 1998, "Experimental study of cellular shedding vortices behind a tapered circular cylinder", *Exp. Thermal Fluid Sci.*, Vol. 17, pp. 179-188.

Jeong, J., and Hussain, F., 1995, "On the identification of a vortex", *J. Fluid Mech.*, Vol. 285, pp. 69-94.

Manhart M., 2004, "A zonal grid algorithm for DNS of turbulent boundary layers", *Computers & Fluids*, Vol. 33, pp. 435-461.

Narasimhamurthy, V. D., Schwertfirm, F., Andersson, H. I., and Pettersen, B., 2006, "Simulation of unsteady flow past tapered circular cylinders using an immersed boundary method", *Proceedings, ECCOMAS European Conference on Computational Fluid Dynamics*, P. Wesseling et al., ed., TU Delft, The Netherlands.

Narasimhamurthy, V. D., Andersson, H. I., and Pettersen, B., 2007, "Direct numerical simulation of vortex shedding behind a linearly tapered circular cylinder", *Proceedings, IUTAM Symposium on Unsteady Separated Flows and their Control*, Corfu, Greece.

Papangelou, A., 1992, "Vortex shedding from slender cones at low Reynolds numbers", *J. Fluid Mech.*, Vol. 242, pp. 299-321.

Parnaudeau, P., Heitz, D., Lamballais, E., and Silvestrini, J. H., 2007, "Direct numerical simulations of vortex shedding behind cylinders with spanwise linear nonuniformity", *J. Turbulence*, Vol. 8, No. 13.

Peller, N., Le Duc, A., Tremblay F., and Manhart M., 2006, "High-order stable interpolations for immersed boundary methods", *Int. J. Numer. Meth. Fluids.* Vol. 52, pp. 1175-1193.

Piccirillo, P. S., and Van Atta, C. W., 1993, "An experimental study of vortex shedding behind linearly tapered cylinders at low Reynolds number", *J. Fluid Mech.*, Vol. 246, pp. 163-195.

Vallès, B., Andersson, H. I., and Jenssen, C. B., 2002, "Oblique vortex shedding behind tapered cylinders", *J. Fluids Struct.*, Vol. 16, pp. 453-463.

Williamson, C. H. K., 1996, "Three-dimensional wake transition", *J. Fluid Mech.*, Vol. 328, pp. 345-407.